DOI: 10.1002/anie.201102628

Artificial Cells

Cytoskeletal-like Supramolecular Assembly and Nanoparticle-Based Motors in a Model Protocell**

*Ravinash Krishna Kumar, Xiaoxiao Yu, Avinash J. Patil, Mei Li, and Stephen Mann**

Reconstitution of cellular functions within synthetic constructs such as lipid or surfactant vesicles represents a central objective of protocell research.[1–4] Realizing this goal has important implications for the design and construction of soft, water-based compartmentalized systems with lifelike properties, and should provide unique opportunities in synthetic biology and bionanotechnology,[5] as well as research on the origins of life.[6] Recent studies have developed synthetic protocell models based on vesicles capable of polymerase chain reaction (PCR) induced DNA amplification,[7] gene expression of single components[8] or cascading networks,[9,10] biochemical transformations,[11] poly(adenylic acid) synthesis,[12] or RNA replication.[13] In contrast, there have been relatively few reports on the reconstitution of dynamically self-assembled cytoskeletal-like structures within protocell models.[14–18] Whilst these studies represent important steps towards the confirmation and refinement of biological mechanisms of cytoskeletal assembly and organization, the possibility of mimicking the cytoskeleton synthetically, that is, using the reversible noncovalent supramolecular assembly of nonbiological components, has not, to the best of our knowledge been explicitly explored. In contrast to previous studies on the encapsulation of polymer gels in vesicles,[20–23] herein we report the noncovalent assembly of a supramolecular network within the interior of phospholipid vesicles using the in situ enzymatic dephosphorylation of small-molecule, amino-acid-based components. Moreover, we exploit supramolecular gelation within the vesicles to generate robust, soft microcompartments capable of chemically derived self-propulsion arising from the platinum-nanoparticle-catalyzed decomposition of hydrogen peroxide (H_2O_2).[24–30]

Aqueous suspensions of 1-palmitoyl-2-oleoyl-*sn*-glycero-3-phosphocholine (POPC) vesicles comprising supramolecular hydrogel interiors were prepared using an inverted emulsion method[31,32] combined with in situ alkaline phosphatase-mediated dephosphorylation of *N*-fluorenylmethyl-carbonyl–tyrosine-(*O*)-phosphate (Fmoc-TyrP; see Scheme 1 in the Supporting Information).[33] As described previously,[33,34] the latter process results in the noncovalent self-assembly of Fmoc-Tyr molecules into bundles of supramolecular nanofilaments that exhibit solid-like viscoelastic properties (see Figure S1 in the Supporting Information), and can be reversibly disassembled by heating the hydrogels above the gel-sol transition temperature (typically around 45 °C). Optical microscopy studies indicated that the amino acid/enzyme-containing hydrogelled vesicles were not aggregated, spherical in shape, 1–25 μm in diameter, and structurally stable when dispersed in water for several months at room temperature, or freeze-dried and investigated by SEM (Figure 1 a,b). The hydrogelled vesicles could be sedimented and rehydrated by slow centrifugation at 120 *g* for 30 minutes, and were relatively stable to changes in osmotic gradients. In contrast, nongelled, water-filled vesicles aggregated after several days

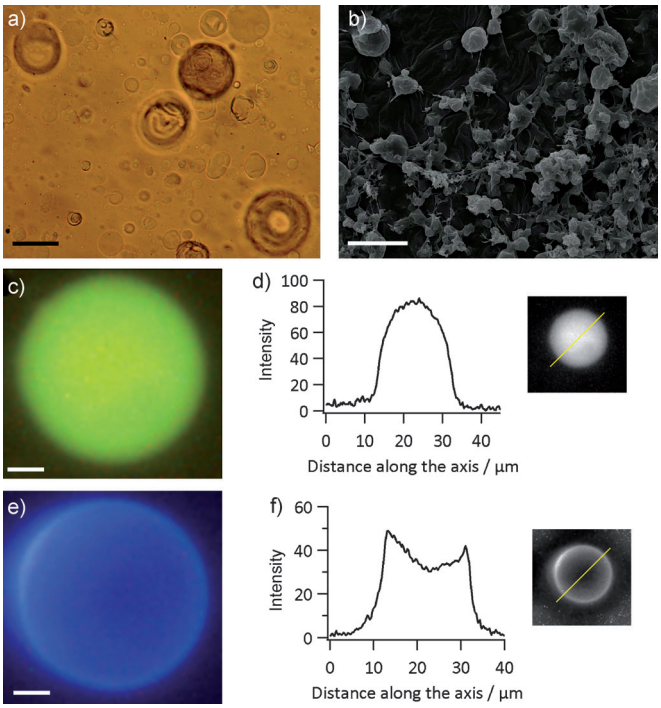

Figure 1. a) Bright-field optical microscopy image of POPC vesicles after in situ supramolecular gelation. The brown coloration arises from the presence of the iron oxide containing protein ferritin, which was co-encapsulated with Fmoc-TyrP and alkaline phosphatase. b) SEM image of vesicles after freeze drying showing gel-like spheroidal microparticles; scale bars: 20 μm. c–f) Fluorescence microscopy images (c,e) and corresponding line-intensity profiles (d,f) of single supramolecular hydrogel vesicles with entrapped calcein (c,d) or membrane-bound TNS (e,f); scale bars: 10 μm.

[*] R. Krishna Kumar, Dr. X. Yu, Dr. A. J. Patil, Dr. M. Li, Prof. S. Mann
Centre for Organized Matter Chemistry, School of Chemistry
University of Bristol, Bristol, BS8 1TS (UK)
E-mail: s.mann@bristol.ac.uk

[**] We thank the EPSRC and the China Scholarship Council (X.Y.) for supporting this study, James Grieve (particle tracking, viscosity measurements), Andy Salmon (aspiration experiments), Stuart Bellamy (optical microscopy), and David Williams (data analysis) for help with experiments, and the Bristol Centre for Nanoscience and Quantum Information and Bristol Wolfson Bioimaging Suite for providing facilities.

Supporting information (including full details of experimental methods) for this article is available on the WWW under http://dx.doi.org/10.1002/anie.201102628.

in aqueous solution, collapsed when examined by scanning electron microscopy (SEM), ruptured when centrifuged, and were sensitive to changes in ionic strength. Fluorescence microscopy images of individual vesicles containing water-soluble calcein or the anionic membrane dye 2-(*p*-toluidinyl)naphthalene-6-sulfonic acid (TNS) confirmed that assembly of the Fmoc-Tyr hydrogel within the interior of the vesicles did not disrupt the surrounding phospholipid bilayer (Figure 1 c–f).

Transmission electron microscopy (TEM) micrographs of partially disrupted vesicles showed the presence of non-branching primary nanofilaments that were on average, approximately 30 nm in width (Figures 2 a,b and Figure S2 in the Supporting Information). The filaments were bundled into larger interconnected fibers that were several micrometers in length to produce a self-assembled amino-acid-based hydrogel network located specifically within the vesicle interior. UV-vis spectra of samples of the Fmoc-Tyr hydrogel (control) and the supramolecular hydrogel vesicles showed three absorption bands centered at 265, 288, and 299 nm, and these bands were attributed to $\pi\rightarrow\pi^*$, $n\rightarrow\pi^*$, and $n\rightarrow\pi^*$ transitions, respectively (Figure 2 c–e).[35] Compared with the aqueous Fmoc-TyrP (Figure 2 c), the Fmoc-Tyr hydrogel showed a characteristic hypochromicity for the absorption band at 265 nm, in contrast with the peak at 299 nm (Figure 2 d); this effect is due to superhelical stacking of the Fmoc groups in the Fmoc-Tyr hydrogel.[36,37] The corresponding change in the A_{265}/A_{299} intensity ratio was almost the same for both the control hydrogel and the supramolecular hydrogel vesicles (Figure 2 c–e; 3.5:1, 3.2:1 and 3.0:1 for the aqueous Fmoc-TyrP, Fmoc-Tyr control gel, and hydrogel vesicles, respectively), indicating that self-assembly of the supramolecular array of Fmoc-modified amino acid molecules was unperturbed by confinement within the phospholipid vesicle interior. This conclusion was consistent with the presence of red-shifted bands corresponding to the amide group, emergence of an absorbance for the phenol moiety, and the disappearance of the signal for the P-O-aryl stretch in the ATR-FTIR spectra (see Figure S3 in the Supporting Information).[34]

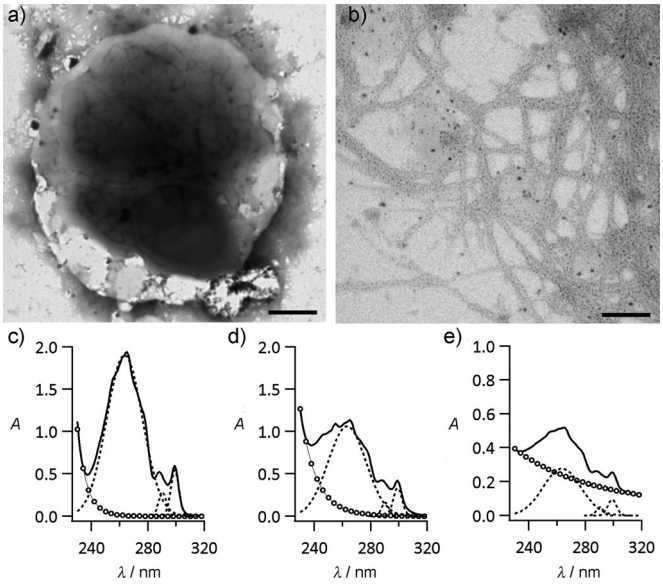

Figure 2. a) Stained TEM image showing a single, partially disrupted POPC vesicle comprising a supramolecular hydrogel core; scale bar = 1 μm. b) High-magnification stained image of an exposed area of the internal hydrogel associated with the vesicle shown in (a); a network of nanofilaments is clearly observed; scale bar = 100 nm. c–e) UV/Vis spectra of a control sample of aqueous Fmoc-TyrP in 100 μM alkaline phosphate buffer (c), a control sample of Fmoc-Tyr hydrogel aged for 24 h after the addition of alkaline phosphatase to 100 μM Fmoc-TyrP/alkaline phosphate buffer (d), and supramolecular hydrogel POPC vesicles after centrifugation and rehydration in alkaline phosphate buffer (e). Plots in (c–e) show raw data (solid lines), background correction (power series) for light scattering (open circles), and multiple Gaussian fits to the raw data after background correction (dashed lines).

Optical tracking was used to determine the viscosity of the vesicle-encapsulated supramolecular hydrogels (see Figure S4 in the Supporting Information). Whereas significant changes in the translational motion of the entrapped fluorescent beads were observed for entrapment in the water-filled vesicles, the microspheres incorporated into the supramolecular hydrogel vesicles remained almost stationary. The respective diffusion constants were 1.34×10^{-13} and $4.78\times10^{-16}\,m^2s^{-1}$, thereby corresponding to nearly a thousand times increase in the viscosity of the hydrogelled vesicles (1.82 Pa s) when compared with the water-filled compartments (0.002 Pa s).

Taken together, the above results were consistent with the formation of vesicles comprising a viscoelastic internal supramolecular matrix of amino-acid-based nanoscale filaments surrounded by a structurally intact phospholipid membrane. This data suggested that in situ supramolecular gelation of the vesicles can be considered a first step towards the construction of model protocells comprising artificial cytoskeletal-like interiors; however we recognize that more realistic models require both internalized structuration and membrane-specific attachment domains. To further develop this paradigm, we investigated the time-dependent deformation behavior of the supramolecular hydrogel vesicles when sedimented against a glass substrate in a sealed chamber and maintained at the gel-sol transition temperature (40 °C) for prolonged periods of time. Compared with water-filled vesicles, which showed no changes in spherical morphology when incubated at 40 °C for 30 minutes (see Figure S5 in the Supporting Information), the hydrogel-containing vesicles underwent a continuous series of dynamic fluctuations to produce a range of transient forms with quasispherical, ellipsoidal, dumbbell, or teardrop morphologies (Figure 3 a). Plots of the time-dependent deformations for individual vesicles indicated that there was a general increase in anisotropy with time from an aspect ratio of 1.0 to a threshold value of around 1.5; however, higher values (2.0–2.5), which rapidly relaxed to lower levels of anisotropy, were occasionally observed (Figure 3 b and see Figure S6 in the Supporting Information,). The dynamic behavior associated with deformations along two specified axes for a given vesicle was also monitored (Figure 3 c). Typically, changes in length along these directions were often minimal for significant periods of

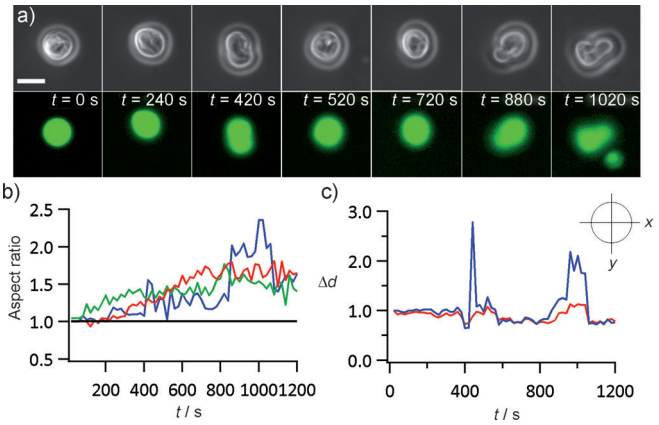

Figure 3. a) Time sequence of phase contrast and fluorescent microscopy images showing dynamical fluctuations in morphology for a supramolecular hydrogel POPC vesicle containing calcein and maintained at 40 °C; scale bar = 10 μm. b) Plots of aspect ratio (long axis/short axis) against time for three individual hydrogel-filled vesicles maintained at 40 °C (blue, red, and green plots). The corresponding data for water-filled POPC vesicles are also shown (black line). c) Plot of relative change in dimension (Δd) along two specified orthogonal directions (x/x_i (blue) and y/y_i (red), where x_i and y_i are initial dimensions at $t = 0$) as a function of time (t) for supramolecular hydrogel vesicles maintained at 40 °C.

time (ca. 400 s), after which there would be a dramatic increase in the changes because of a considerable outward expulsion of the lipid bilayer that could last for periods of several hundred seconds before relaxation back to the steady-state value. These events occurred intermittently, and often a few times over the time period of the observations.

The above results suggested that the hydrogel interior of the vesicles becomes heterogeneous when maintained at the gel-sol transition temperature. One possibility is that anisotropy in the mechanical properties of the internal network is generated by preferentially melting the disordered regions of the supramolecular network to produce a viscoelastic matrix consisting of microdomains of relatively stiff, highly ordered nanofilaments dispersed in a fluid of disassembled Fmoc-Tyr monomers. This proposal was consistent with the differential scanning calorimetry (DSC) data, which showed a broad gel-sol transition (see Figure S7 in the Supporting Information). Given this heterogeneity, thermal fluctuations as well as osmotic pressure changes could then result in dynamic changes in shape deformation resulting from localized movements of the sol and gel components within the vesicle core. Although the vesicles were not motile, the dynamic extensions and relaxations around their boundary implied that the structural integrity and fluidity of the surrounding bilayer membrane were not only intact but also served to attenuate the morphological deformations, as evidenced by the limiting aspect ratio determined by optical imaging. Interestingly, cooling the deformed vesicles to room temperature did not restore the spherical isotropic shape (see Figure S8 in the Supporting Information), but instead kinetically trapped the morphological anisotropy produced at 40 °C.

As supramolecular gelation within the vesicles gave rise to a considerable increase in the robustness of the microcompartments—for example they could be supported as nondeformable microspheres against an aspirator pipette under negative pressure (see Figure S9 in the Supporting Information)—it seemed feasible that such structures could be exploited for the development of protocell models exhibiting chemically derived motility and self-propulsion. As proof-of-concept, we demonstrated this by electrostatically binding positively charged platinum nanoparticles (see Figure S10 in the Supporting Information) to the outer membrane surface of the supramolecular hydrogel vesicles—the respective zeta potentials at neutral pH before mixing were +31.7 and −10.8 mV—with subsequent addition of hydrogen peroxide as a fuel. TEM images and energy dispersive X-ray analysis showed that addition of the colloid resulted in hydrogelled vesicles with a nonuniform surface coating of discrete platinum nanoparticles (see Figure S11 in the Supporting Information). The autonomous motion of the platinum-coated vesicles was monitored by optical tracking of samples placed in a sealed enclosure containing a 30 μm-thick layer of aqueous hydrogen peroxide (30 wt %). Introduction of the vesicles into the chamber resulted in immediate movement, often along quasilinear trajectories that covered a distance of 70–100 μm during the initial 10 seconds (Figure 4a). No movement was observed without the addition of hydrogen peroxide. Similarly, vesicles with hydrogel interiors remained stationary in the absence of the surface-adsorbed platinum nanoparticles. Significantly, the motility was readily tracked because the trajectories were elaborated by a stream of persistent gas bubbles with high optical contrast (Figure 4a). Video recordings indicated that translational movement of the vesicles effectively stopped after the initial 10 second burst, with subsequent intermittent locomotion at reduced speeds along with changes in direction over a period of 100 seconds (Figure 4b,c). After the initial 10 seconds, the vesicle speed typically oscillated aperiodically (Figure 4d), with an average speed of 2.5–3 $\mu m\,s^{-1}$, which corresponds to a viscous drag of 0.26 pN for a vesicle of 5 μm radius. Overall, the results suggested that stochastic fluctuations in the H_2O_2 diffusion gradient associated with fuel consumption at the nonuniformly coated vesicle membrane were responsible for the intermittent movement.

In conclusion, we have demonstrated that an amino-acid-based supramolecular hydrogel can be noncovalently assembled within phospholipid vesicles by in situ enzyme-mediated dephosphorylation to produce viscoelastic interiors comprising a confined network of Fmoc-Tyr nanofilaments. Significantly, the supramolecular hydrogel vesicles show dynamic behavior in their modes of morphological deformation when incubated for prolonged periods at 40 °C as compared to water-filled vesicles that remain shape-invariant. We also demonstrate that platinum nanoparticles can be attached to the outer surface of the bilayer membrane and exploited for the autonomous movement of the supramolecular hydrogel vesicles. Taken together, our results point the way forward to the construction of new types of model protocells with synthetic cytoskeletal-like supramolecular architectures and externally located nanoparticle-based motors. Such constructs could be further developed for the fabrication of robust and motile artificial cell-like entities for use in areas such as

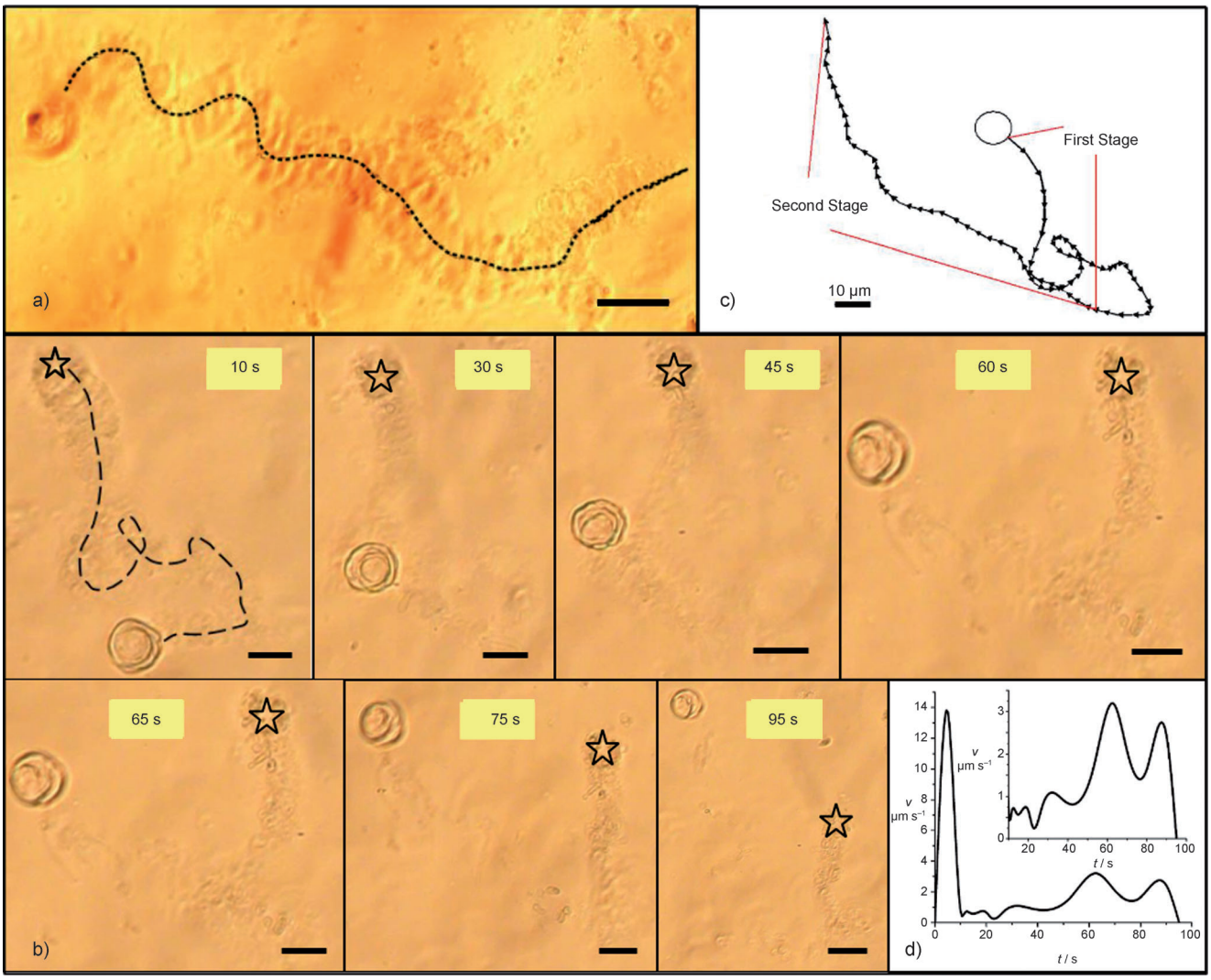

Figure 4. Optical tracking of autonomous motion for platinum-nanoparticle-coated supramolecular hydrogel vesicles in the presence of aqueous H_2O_2 at various time intervals after mixing. The vesicles were prepared from the phospholipid 1,2-dimyristoyl-*sn*-glycero-3-phosphocholine (DMPC). a) Image recorded after 10 s showing gas bubble track marking the trajectory (dotted line) of a single vesicle from the right- to left-hand side of the photograph. Scale bar = 10 µm. b) Video stills showing trajectory of a single vesicle between 0–100 s. The path taken during the initial burst in locomotion in the first 10 s is shown as a dotted line. The asterisk represents the starting point prior to movement. Scale bars = 10 µm. c) Plot of the trajectories observed in (b) showing the rapid first stage and slower second stage in locomotion. d) Plot of velocity with time (0–100 s) for the movement of a single platinum-nanoparticle-coated supramolecular hydrogel vesicle in the presence of H_2O_2; inset shows magnified profile for time interval between 10–100 s.

synthetic biology, remote sensing, and microscale bioreactor processing.

Received: April 15, 2011
Revised: May 19, 2011
Published online: July 18, 2011

Keywords: artificial cells · nanoparticles · self-assembly · sol-gel processes · vesicles

[1] *Protocells: Bridging Nonliving and Living Matter*. (Ed.: S. Rasmussen, M. A. Bedau, L. Chen, D. Deamer, D. C. Krakauer, N. H. Packard, P. F. Stadler), MIT Press, Cambridge USA, **2009**.
[2] J. W. Szostak, D. P. Bartel, P. L. Luisi, *Nature* **2001**, *409*, 387–390.
[3] P. L. Luisi, *The Emergence of Life*, Cambridge University Press, Cambridge, **2006**.
[4] S. S. Mansy, J. P. Schrum, M. Krishnamurthy, S. Tobé, D. A. Treco, J. W. Szostak, *Nature* **2008**, *454*, 122–125.
[5] A. Porhorille, D. Deamer, *Trends Biotechnol.* **2002**, *20*, 123–128.
[6] J. P. Schrum, T. F. Zhu, J. W. Szostak, *Cold Spring Harbor Perspect. Biol.* **2010**, *2*, a002212.
[7] T. Oberholzer, M. Albrizio, P. L. Luisi, *Chem. Biol.* **1995**, *2*, 677–682.
[8] S. M. Nomura, K. Tsumoto, T. Hamada, K. Akiyoshi, Y. Nakatani, K. Yoshikawa, *ChemBioChem* **2003**, *4*, 1172–1175.
[9] K. Ishikawa, K. Sato, Y. Shima, I. Urabe, T. Yomo, *FEBS Lett.* **2004**, *576*, 387–390.
[10] V. Noireaux, A. Libchaber, *Proc. Natl. Acad. Sci. USA* **2004**, *101*, 17669–17674.
[11] P. Walde, S. Ichikawa, *Biomol. Eng.* **2001**, *18*, 143–177.

[12] P. Walde, A. Goto, P. A. Monnard, M. Wessicken, P. L. Luisi, *J. Am. Chem. Soc.* **1994**, *116*, 7541 – 7547.
[13] T. Oberholzer, R. Wick, P. L. Luisi, C. K. Biebricher, *Biochem. Biophys. Res. Commun.* **1995**, *207*, 250 – 257.
[14] D. A. Fletcher, R. D. Mullins, *Nature* **2010**, *463*, 485 – 492.
[15] A. P. Liu, D. A. Fletcher, *Nat. Rev. Mol. Cell Biol.* **2009**, *10*, 644 – 650.
[16] L. Limozin, E. Sackmann, *Phys. Rev. Lett.* **2002**, *89*, 168103.
[17] L.-L. Pontani, J. Gucht, G. Salbreux, J. Heuvingh, J.-F. Joanny, C. Sykes, *Biophys. J.* **2009**, *96*, 192 – 198.
[18] V. Delatour, E. le Helfer, D. Didry, K. H. D. Le, J.-F. Gaucher,, M.-F. Carlier, G. R. Lemonne, *Biophys. J.* **2008**, *94*, 4890 – 4905.
[19] H. Hotani, T. Inaba, F. Nomura, S. Takeda, K. Takiguchi, T. J. Itoh, T. Umeda, A. Ishijima, *Biosystems* **2003**, *71*, 93 – 100.
[20] A. Viallat, J. Dalous, M. Abkarian, *Biophys. J.* **2004**, *86*, 2179 – 2187.
[21] A. Jesorka, M. Markström, M. Karlsson, O. Orwar, *J. Phys. Chem. B* **2005**, *109*, 14759 – 14763.
[22] M. Faivre, C. C. Campillo, B. Pépin-Donat, A. Viallat, *Prog. Colloid Polym. Sci.* **2006**, *133*, 41 – 44.
[23] C. C. Campillo, A. P. Schroder, C. M. Marques, B. Pépin-Donat, *Mater. Sci. Eng. C* **2009**, *29*, 393 – 397.
[24] R. F. Ismagilov, A. Schwartz, N. Bowden, G. M. Whitesides, *Angew. Chem.* **2002**, *114*, 674 – 676; *Angew. Chem. Int. Ed.* **2002**, *41*, 652 – 654.
[25] W. F. Paxton, P. T. Baker, T. R. Kline, Y. Wang, T. E. Mallouk, A. Sen, *J. Am. Chem. Soc.* **2006**, *128*, 14881 – 14888.
[26] W. F. Paxton, A. Sen, T. E. Mallouk, *Chem. Eur. J.* **2005**, *11*, 6462 – 6470.
[27] T. R. Kline, W. F. Paxton, T. E. Mallouk, A. Sen, *Angew. Chem.* **2005**, *117*, 754 – 756; *Angew. Chem. Int. Ed.* **2005**, *44*, 744 – 746.
[28] J. M. Catchmark, S. Subramanian, A. Sen, *Small* **2005**, *1*, 202 – 206.
[29] D. Pantarotto, W. R. Browne, B. L. Feringa, *Chem. Commun.* **2008**, 1533 – 1535.
[30] J. Vicario, R. Eelkema, W. R. Browne, A. Meetsma, R. M. La Crois, B. L. Feringa, *Chem. Commun.* **2005**, 3936 – 3938.
[31] S. Pautot, B. J. Frisken, D. A. Weitz, *Langmuir* **2003**, *19*, 2870 – 2879.
[32] A. Campbell, P. Taylor, O. J. Cayre, V. N. Paunov, *Chem. Commun.* **2004**, 2378 – 2379.
[33] Z. Yang, H. Gu, D. Fu, P. Gao, J. K. Lam, B. Xu, *Adv. Mater.* **2004**, *16*, 1440 – 1444.
[34] Z. A. C. Schnepp, R. Gonzalez-McQuire, S. Mann, *Adv. Mater.* **2006**, *18*, 1869 – 1872.
[35] M. N. R. Ashfold, B. Cronin, A. Devine, R. Dixon, M. Nix, *Science* **2006**, *312*, 1637 – 1640.
[36] K. Channon, G. Devlin, S. Magennis, C. Finlayson, A. Tickler, C. Silvia, C. MacPhee, *J. Am. Chem. Soc.* **2008**, *130*, 5487 – 5491.
[37] D. M. Ryan, T. M. Doran, B. L. Nilsson, *Chem. Commun.* **2011**, *47*, 475 – 477.